RSC Sustainability

ROYAL SOCIETY OF CHEMISTRY

PAPER

View Article Online
View Journal | View Issue

Cite this: *RSC Sustainability*, 2025, **3**, 3520

Effects of alkanolamines on photocatalytic reduction of carbon dioxide to liquid fuels using a copper-doped dititanate/graphene photocatalyst†

Wannisa Neamsung,[a] Nutkamol Kitjanukit,[a] Apisit Karawek,[a] Napatr Chongkol,[a] Napat Lertthanaphol,[ab] Poomipat Chotngamkhum,[a] Kongphoom Khumsupa,[a] Poomiwat Phadungbut,[a] Woranart Jonglertjunya,[a] Pattaraporn Kim-Lohsoontorn[c] and Sira Srinives *[a]

Carbon dioxide (CO_2) photoreduction is a promising alternative to carbon capture, utilization, and storage (CCUS) technologies. It relies on photocatalysts to convert CO_2 to high-value products. The copper-doped dititanate nanosheets/graphene oxide composite (CTGN) is a heterostructure of two 2-dimensional nanomaterials: nanosheets and graphene oxide (GO), exhibiting outstanding photoactivity. It was demonstrated to assist in CO_2 photoreduction, yielding fuel products such as methanol, ethanol, and isopropanol. In this study, we used CTGN as a photocatalyst model to investigate the effects of alkanolamines, including monoethanolamine (MEOA), diethanolamine (DEOA), and triethanolamine (TEOA), in facilitating CO_2 photoreduction. TEOA performed the best, producing methanol, ethanol, isopropanol, acetone, and *n*-butanol with an impressive total carbon consumption (TCC) of 7890 μmol g_{cat}^{-1}. Alkanolamines exhibited a dual function as a sacrificial agent (SCR) and a CO_2-capturing substance for photoreduction. TEOA was an excellent SCR and captured CO_2 loosely *via* base-catalyzed hydration, promoting the subsequent release of CO_2 for photoreduction. A study on medium pH revealed a decreased photoreduction rate at increased pH due to a strong bond between CO_2 and the alkali solution, which reduces the reaction rate.

Received 11th April 2025
Accepted 23rd June 2025

DOI: 10.1039/d5su00268k

rsc.li/rscsus

Sustainability spotlight

CO_2 is a greenhouse gas and a primary contributor to climate change. It contributes to rising global temperatures and has a significant impact on ecosystems. CO_2 photoreduction is an emerging technique that has earned the name 'artificial leaf' due to its reliance on UV light and CO_2. It relies on photocatalysts to transform CO_2 into high-valued substances, such as fuels and industrial feedstocks. Herein, we have used three alkanolamines, MEOA, DEOA, and TEOA, as facilitators in CO_2 photoreduction with CTGN as a photocatalyst. The alkanolamines increased dissolved CO_2 concentration in the medium and promoted the electron-hole separation of the photocatalysts. Our efforts to encourage CO_2 emission reduction align with the UN's Sustainable Development Goals of affordable and clean energy (SDG 7) and climate action (SDG 13).

Introduction

The global trend in climate change, global warming, and CO_2 emission reduction has advanced the development of CCUS technologies. The current and latest CCUS technologies include the capture of CO_2 gas using an amine scrubber,[1,2] a solid adsorbent,[3,4] a membrane separator,[5,6] and a cryogenic system.[7,8] Alternative technologies have advanced significantly over the past few decades. Examples include storing CO_2 in biological and geological systems (such as oceans, forests, and underground spaces),[9–11] direct air capture (DAC),[12] and the catalytic conversion of CO_2 into other high-value products.[13–16] These inventions were developed and demonstrated for industrial use but needed further development and investment.

Catalytic conversion of CO_2 is an intriguing approach that captures CO_2 and yields high-value products for use in industry or for sale. Titanium dioxide (TiO_2) is a photocatalyst recognized for its ability to treat water and coat surfaces. It was demonstrated for CO_2 photoreduction.[17–19] A typical mechanism

[a]*Nanocomposite Engineering Laboratory (NanoCEN), Department of Chemical Engineering, Faculty of Engineering, Mahidol University, Nakhon Pathom 73170, Thailand. E-mail: ssrinives@gmail.com*

[b]*Chemical Engineering Department, University of Louisville, Louisville, KY 40292, USA*

[c]*Centre of Excellence on Catalysis and Catalytic Reaction Engineering (CECC), Department of Chemical Engineering, Faculty of Engineering, Chulalongkorn University, Bangkok 10330, Thailand*

† Electronic supplementary information (ESI) available. See DOI: https://doi.org/10.1039/d5su00268k

involves the activation of TiO_2 by light, generating photoelectrons and photo-induced holes. The photoelectrons transfer from the valence band (VB) to the conductive band (CB) and are incorporated with CO_2. The incorporation yields a CO_2^{*-} radical that is an intermediate in product generation.[20,21] For a photocatalyst to generate photoelectrons constantly, the photo-induced holes in the VB must stay separated from the photoelectrons by reacting with the hole-scavenging SCR. Examples of SCRs include water, alcohols, amines, and biomass.[22–27] Water is the most common SCR to withdraw holes from photocatalysts and form hydroxyl ions (OH^-). The SCR performance relies on the chemical properties of the substance, including its polarity, diffusivity, interactions with the catalyst surface, and nucleophilicity.

Alkanolamines are a group of amines that contain both amino and hydroxyl moieties. They have been employed in industrial amine scrubbers for the adsorption of CO_2. The amine–CO_2 reaction/interaction follows the paths of acid/base reaction (eqn (1) and (2)) and base-catalyzed hydration (eqn (3) and (4)). The former requires a direct reaction between CO_2 (acid) and two amines (base) to create a carbamate. The latter depends on weak CO_2–amine electrostatic charge interactions that facilitate carbonic acid generation with no amine being spent. The primary and secondary amines prefer the acid–base reaction path, while a tertiary amine undergoes the base-catalyzed hydration path.

Acid–base reaction

$$2RNH_2 + CO_2 \leftrightarrow RNH_3^+ + RNHCOO^- + \text{heat} \quad (1)$$

$$2R_1R_2NH + CO_2 \leftrightarrow R_1R_2NH_2^+ + R_1R_2NCOO^- + \text{heat} \quad (2)$$

Base-catalyzed hydration

$$R_1R_2NH + CO_2 + H_2O \leftrightarrow R_1R_2NH_2^+ + HCO_3^- + \text{heat} \quad (3)$$

$$R_1R_2R_3N + CO_2 + H_2O \leftrightarrow R_1R_2R_3NH^+ + HCO_3^- + \text{heat} \quad (4)$$

Alkanolamines offer dual functionalities as a CO_2-capturing substance and an SCR and have been studied for CO_2 photoreduction. For instance, Liao Y and team[28] synthesized TiO_2 particles using a solvothermal technique and modified TiO_2 with MEOA. MEOA/TiO_2 exhibited four times the CO_2 adsorption capacity and photoreduction rate compared to a bare TiO_2. MEOA enhanced CO_2–TiO_2 interactions by attracting CO_2 to the proximity of TiO_2, which promoted photoreduction. The group of Kim Y. E.[29] studied CO_2-capturing performances of MEOA, DEOA, and TEOA. MEOA and DEOA reacted with CO_2 through the acid–base reaction (eqn (1) and (2)), and DEOA and TEOA interacted with CO_2 through the base-catalyzed hydration (eqn (3) and (4)). MEAO required more heat for CO_2 absorption than DEOA and TEOA, while DEOA provided more CO_2 loading capacity than MEOA and TEOA. Karawek A. and team[22] modified TiO_2 nanosheets with MEOA, DEOA, and TEOA and used the nanosheets to assist CO_2 photoreduction. TEOA/TiO_2 showed the best photoactivity since TEOA underwent the base-catalyzed hydration with CO_2. The hydration generated carbonic acid, which could effectively be used in the following photoreduction.

Our group synthesized CTGN and studied its photoactivity for CO_2 photoreduction.[17,19] Letthanaphol N[19] tested CTGN with water SCR in CO_2 photoreduction and reported the formation of target products, including methanol, ethanol, isopropanol, and acetone. The key to good photoactivity is the n–p heterojunction interfaces between the dititanate nanosheets and GO, which direct the path for charge mobility. Kitjanukit N.[17] studied the effects of alcohol SCRs, including methanol, ethanol, and isopropanol, on CO_2 conversion using a CTGN photocatalyst. Methanol SCR yielded the highest product generation rate due to its small molecular size, which resulted in high mass diffusivity and an improved hole scavenging ability.

In this work, we investigated the effects of MEOA, DEOA, and TEOA on the CO_2 photoreduction. CTGN was used as a photocatalyst model. The liquid samples from the photoreduction were collected and analyzed by gas chromatography (GC) to determine their molar compositions. CTGN was also characterized to demonstrate consistency in material synthesis using transmission electron microscopy (TEM), field-emission scanning electron microscopy (FE-SEM), Fourier transform infrared (FTIR) spectroscopy, Raman spectroscopy, and X-ray diffraction (XRD).

Experimental

All chemicals used in the experiment were purchased and used without further purification. For GO synthesis, graphite flakes (99.9%, AR grade, Alfa Aesar, 325 mesh, USA), sulfuric acid (AR grade, RCI Labscan, 98% H_2SO_4, Thailand), sodium nitrate (AR grade, Fluka chemika, 99% $NaNO_3$, Switzerland), potassium permanganate (AR grade, Ajax Finechem, 99% $KMnO_4$, Australia), hydrogen peroxide (AR grade, Merck, 30% H_2O_2, Germany), and hydrochloric acid (AR grade, RCI Labscan, 37% HCl, Thailand) were used. CTGN production required other chemicals: sodium hydroxide (AR grade, Ajax Finechem, NaOH, Australia), titanium(IV) butoxide (AR grade, Sigma Aldrich, TBOT, 97% $Ti(OCH_2CH_2CH_2CH_3)_4$, Germany), ethanol (AR grade, RCI Labscan, 99.9% C_2H_5OH, Thailand), and copper(II) nitrate (AR grade, Sigma Aldrich, $Cu(NO_3)_2 \cdot 3H_2O$, New Zealand). MEOA (AR grade, 99% C_2H_7NO (Table 1)) and DEOA (AR grade, 99% $C_5H_{11}NO_2$ (Table 1)) were purchased from TCI

Table 1 Molecular formulation, p*K*a, and relative permittivity (dielectric constant) values of MEOA, DEOA, and TEOA

No.	Name	pK_a	Relative permittivity	Structure
1	MEOA	9.44	31.9 (ref. 30)	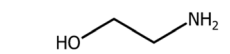
2	DEOA	8.88	25.8 (ref. 30)	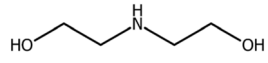
3	TEOA	7.72	29.3 (ref. 31)	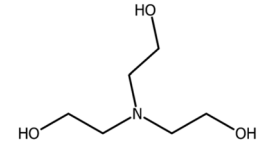

Japan, while TEOA (AR grade, TEOA, 99% $C_6H_{15}NO_3$ (Table 1)) was purchased from Ajax Finechem Australia. CO_2 gas was 99.9% pure and purchased from Lor Ching Tong Oxygen, Thailand.

CTGN characterization studies

Complete characterization studies of CTGN were provided in our previous work,[17–19] and they are only offered here to verify the reliability of the synthesis method. Surface morphology was observed using TEM (HR-TEM, Tecnai 20 Philips instrument). FTIR (JASCO FT/IR-6800) was used to study chemical functionalities from IR responses within the 400–4000 cm^{-1} range. Optical properties were investigated using a UV-vis spectrophotometer (UV-vis, 1800 SHIMADZU), where light absorbance was analyzed and optical bandgap energy was determined. The crystal structure was examined using X-ray diffraction (XRD, Bruker D2 PHASER) with Cu Kα radiation within the 5–80° range and with a scanning rate of 0.02° s^{-1}.

GO synthesis

The chemical exfoliation method was employed to synthesize GO. The synthesis began by mixing 2 g of graphite flakes, 1 g of $NaNO_3$, and 50 mL of concentrated H_2SO_4 acid in a 250 mL flask. The mix was kept at a temperature below 4 °C in an ice bath with stirring for 2 h and then blended with 10 g of $KMnO_4$. The flask was removed from the bath to keep it under ambient conditions and stirred for 2 h. At this point, the graphite was oxidized to GO. The reaction was terminated by adding 20 mL of 30% v/v H_2O_2 to the mix, yielding a yellow-brown suspension of GO. The powder was filtered using a vacuum filtration apparatus with microfilter paper (GF/C, Whatman). The GO slurry was rinsed with a 3% v/v HCl solution, followed by DI water using a centrifuge machine (Eppendorf 5804R laboratory centrifuge). GO powder was dried in a vacuum oven (Faithful Instrument (HEBE) Co., Ltd) at 60 °C for 24 h and stored in a desiccator for future use.

Synthesis of CTGN and control samples

TBOT and $Cu(NO_3)_2$ solutions were prepared separately. We mixed 0.71 mL of TBOT with 20 mL of ethanol and 10 mL of DI water and dissolved $Cu(NO_3)_2$ in DI water at a concentration of 1 mg mL^{-1}. The $Cu(NO_3)_2$ solution was poured into the TBOT solution, and 10 mL of 1 M NaOH solution was added. The mix was blended with GO solution (1.5 mg mL^{-1}) and transferred to a hydrothermal reactor. The reactor was heated at 180 °C for 8 h. The resulting CTGN powder was dried in an oven at 70 °C for 8 h before being stored in a desiccator. Control samples, including dititanate nanosheets (TiNs) and copper-doped dititanate nanosheets (CTNs), were synthesized following a similar hydrothermal technique for comparison. The TiN was synthesized by mixing a solution of TBOT in ethanol with DI water and NaOH solution. The mix was heated at 180 °C for 8 h in a hydrothermal reactor. The CTN was obtained by mixing TBOT and $Cu(NO_3)_2$ solutions with a NaOH solution and heating the blend at 180 °C for 8 h. Dititanate nanosheet/GO (TGN) refers to the CTGN composite without copper, synthesized through a hydrothermal process involving a mixture of TBOT, NaOH, and GO.

CO_2 photoreduction experiments

The effects of MEOA, DEOA, and TEOA SCR on CO_2 photoreduction were investigated by monitoring the production of target substances, including acetaldehyde, methanol, ethanol, isopropanol, and *n*-butanol. A suspension of CTGN was prepared in a 30 mL quartz reactor at a concentration of 0.1 mg mL^{-1} and purged with a pure CO_2 stream at a flow rate of 0.2 L min^{-1} for 20 min. MEOA, DEOA, or TEOA was added to the suspension (0.5 mM). The mix was stirred continuously and illuminated with a 160-watt mercury lamp (Philips). The photoreduction lasted for 6 h before the liquid and gas samples were collected using filtered syringes. The samples were analyzed using gas chromatography (GC) with a DB-WAX column and a flame ionization detector (FID) to determine their composition.

Results and discussion

CTGN characterization studies

The surface morphology of the CTGN was analyzed by TEM, which shows that it has a nanosheet structure of 93.19 ± 21.55 × 57.93 ± 16.48 nm^2 size (Fig. 1(a)), attached to the GO sheet

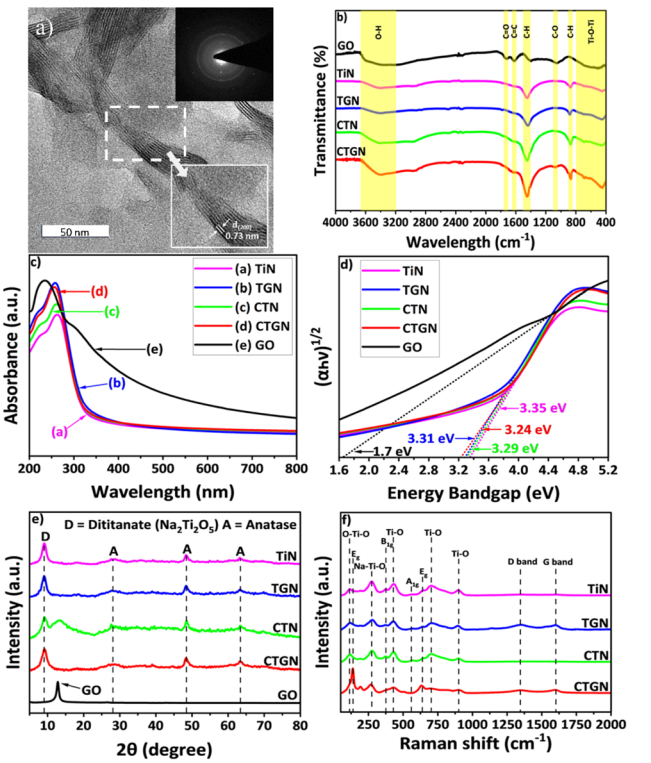

Fig. 1 (a) TEM image showing the physical morphology, lattice space (top inset), and light diffraction pattern (bottom inset) of the CTGN, (b) FTIR spectra of GO, TiN, TGN, CTN, and CTGN, (c) UV-vis spectra and (d) Tauc's plots of TiN, TGN, CTN, and CTGN, (e) XRD patterns of GO, TiN, TGN, CTN, and CTGN, and (f) Raman spectra of TiN, TGN, CTN, and CTGN.

(~15 × 20 μm^2 (Fig. S1†)). The lattice space (Fig. 1(a), bottom inset) was measured as 0.731 nm (Fig. S2†), corresponding to the distance between the {200} planes of sodium dititanate ($Na_2Ti_2O_5$).[17,19] Light diffraction analysis (Fig. 1(a), top inset) revealed a combination of ring and dot patterns, suggesting a mix of polycrystalline and single-crystal structures. FTIR spectra (Fig. 1(b)) showed the IR transmittance of the chemical functionality of the samples. The spectra for GO peaked at 3420, 1730, 1620, 1410, and 1050 cm^{-1}, corresponding to O–H stretching, C=O stretching, C=C aromatic stretching, O–H bending, and C–O stretching, respectively. TiN and CTN exhibited IR spectrum peaks at 3420, 1450, 900, and 400 cm^{-1}, corresponding to O–H stretching, C–H bending, C–H stretching, and Ti–O–Ti or Ti–O–C, respectively. TGN and CTGN exhibited similar transmittance peaks at 3420, 1450, 900, and 400 cm^{-1}, attributed to the signals of O–H stretching, C–H bending, C–H stretching, and Ti–O–Ti or Ti–O–C, respectively.[21] CTGN presented two additional peaks at 1620 and 1050 cm^{-1}, which are attributed to C=C aromatic stretching and C–O stretching due to the presence of GO. Optical properties were studied using a UV-visible spectrophotometer, in which light absorption was monitored from powder suspensions (Fig. 1(c)). Absorption spectra for GO, TiN, TGN, CTN, and CTGN showed maxima at 230, 263, 258, 260, and 256 nm, respectively. The bandgap energy determined by Tauc's correlation (Fig. 1(d)) was 1.7, 3.35, 3.31, 3.29, and 3.24 eV, respectively. XRD (Fig. 1(e)) provided the crystal structure analysis. GO yielded a sharp diffraction peak at 12.82°, which was ascribed to {001} of the graphitic lattice plane. For TiN and CTN, a diffraction peak at 9.20° represented the {200} plane of dititanate, while peaks at 28.08°, 48.38°, and 63.50° corresponded to the {101}, {200} and {204} planes of anatase TiO_2, respectively. TGN and CTGN exhibited similar patterns to TiN, with a peak at 9.20° indexed to the {200} plane of dititanate and peaks at 28.08°, 48.38°, and 63.50° related to the {101}, {200} and {204} planes of anatase TiO_2, respectively. The crystallite sizes were determined using Scherrer's equation and were 10.88, 5.28, 5.23, 5.13, and 5.30 nm for GO, TiN, TGN, CTN, and CTGN, respectively. The large crystallite size of CTGN indicated an extensive grain size and more crystalline structure compared to TiN, TGN, and CTN.[19,21] Raman spectra (Fig. 1(f)) for TiN and CTN presented absorption peaks for O–Ti–O (114.27 cm^{-1}), Na–Ti–O (271.11 cm^{-1}), and Ti–O (436.04, 704.04, and 898.48 cm^{-1}), indicating the existence of dititanate and TiO_2. Small and medium absorption bands revealed the presence of B1g (377.02 cm^{-1}), A1g (566.20 cm^{-1}), and Eg (639.77 cm^{-1}) of TiO_2 anatase. TGN and CTGN exhibited similar trends in Raman spectra, yielding signals for dititanate and anatase TiO_2.[19] The D and G bands from defective and crystalline graphite were observed at 1350 and 1610 cm^{-1}, indicating the presence of GO in the catalysts. The I_D/I_G ratios of 0.841 and 0.843 were calculated for TGN and CTGN, respectively.

CO_2 photoreduction results

CO_2 photoreduction experiments were conducted in a CO_2-saturated CTGN suspension containing 0.5 mM alkanolamine (MEOA, DEOA, or TEOA). A control experiment was performed in a CO_2-saturated CTGN suspension with no alkanolamine (pH ~5). In all the alkanolamine cases, the suspension pH was monitored to be ~7 after CO_2 dissolution. The product compositions were measured using GC analysis and reported as the product generation rate (μmol g_{cat}^{-1} h^{-1}). Preliminary tests revealed the target products of acetaldehyde, methanol, ethanol, isopropanol, acetone, and *n*-butanol. The total carbon consumption (TCC) was determined using eqn (5).

$$\begin{aligned}\text{TCC} = [&(\text{acetaldehyde production rate} \times 2)\\ &+ (\text{methanol production rate} \times 1)\\ &+ (\text{ethanol production rate} \times 2)\\ &+ (\text{isopropanol production rate} \times 3)\\ &+ (n\text{-butanol production rate} \times 4)\\ &+ (\text{acetone production rate} \times 3)] \times 6\end{aligned} \quad (5)$$

TCC indicates the number of carbon atoms in target products obtained from each operation and is used to compare the effects of alkanolamines on the photoreduction rate. For the control experiment (no alkanolamine), CO_2 photoreduction yielded 20, 0, 113, 20, and 0 μmol g_{cat}^{-1} h^{-1} acetone, methanol, ethanol, isopropanol, and *n*-butanol, respectively (Fig. 2). The TCC was determined to be 2086 μmol g_{cat}^{-1}. For MEOA and DEOA, production rates for acetone, methanol, ethanol, isopropanol, and *n*-butanol were 19 and 20, 39 and 37, 158 and 112, 34 and 28, and 2 and 3 μmol g_{cat}^{-1} h^{-1}, respectively. The TCC increased to 3130 and 2424 μmol g_{cat}^{-1}. TEOA exhibits the best results in supporting photoreduction, yielding acetone, methanol, ethanol, isopropanol, and *n*-butanol at 56, 113, 281, 152, and 4 μmol g_{cat}^{-1} h^{-1}, respectively, and a TCC of 7890 μmol g_{cat}^{-1}.

Based on the photoreduction results, the photoreduction quantum efficiency (PQE) was determined using eqn (6),

$$\text{PQE}\ (\%) = \frac{n_e \times \text{production formation rate}\ (\mu\text{mol s}^{-1})}{\text{incident photon rate}\ (\mu\text{mol s}^{-1})} \times 100, \quad (6)$$

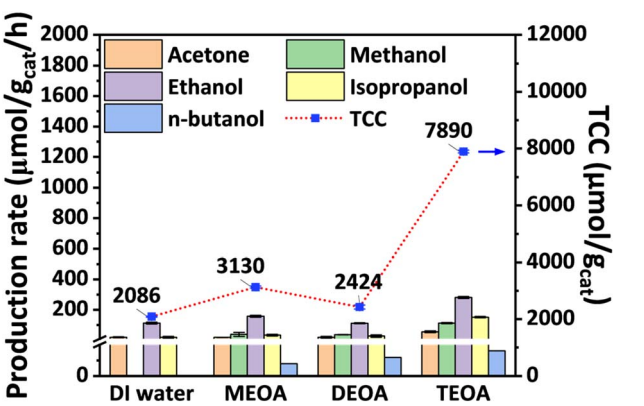

Fig. 2 Production rates and TCCs, corresponding to DI water, MEOA, DEOA, and TEOA SCRs (solution pH ~5 in DI water and ~7 with an alkanolamine).

where n_e denotes the number of electrons needed for the formation of a photoreduction product. The incident photon rate was determined using eqn (7),

$$\text{Incident photon rate } (\mu\text{mol s}^{-1}) = \frac{\text{light intensity (W cm}^{-2}) \times \lambda \text{ (m)} \times \text{A (cm}^2)}{\text{Planck's constant (J s mol}^{-1}) \times \text{photon density (m s}^{-1}) \times \text{Avogadro's number (mol)}} \quad (7)$$

where light intensity is 0.0146 W cm^{-2} (Sanwa LX20 Illuminance meter, diameter 9 mm), λ is the light wavelength (360 nm), A is the projected area on the photochemical cell (12 cm^2), Planck's constant is 6.63 × 10^{-34} J s mol^{-1}, photon density is 3 × 10^8 m s^{-1}, and Avogadro's number is 6.023 × 10^{23} mol.[21,32] The % PQEs of 0.0386, 0.0945, 0.0766, and 0.3693 were determined for water, MEOA, DEOA, and TEOA, respectively (Fig. 3(a)). The highest PQE indicates that photons from light contribute most effectively to photoelectron production in the case of TEOA. The PQE trends agree with the CO_2 photoreduction results. The CO_2 conversion (Fig. 3(b)) was determined using eqn (8),[19]

$$CO_2 \text{ conversion } (\%) = \frac{(CO_2 \text{ solubility} - \text{TCC})}{CO_2 \text{ solubility}} \times 100, \quad (8)$$

in which CO_2 solubility is roughly 33 mM under ambient conditions. The conversions are 93.67, 90.52, 92.66, and 76.09% for water, MEOA, DEOA, and TEOA, respectively. The CTGN demonstrated enhanced photoactivity with TEOA as the facilitator, compared to other alkanolamines and water.

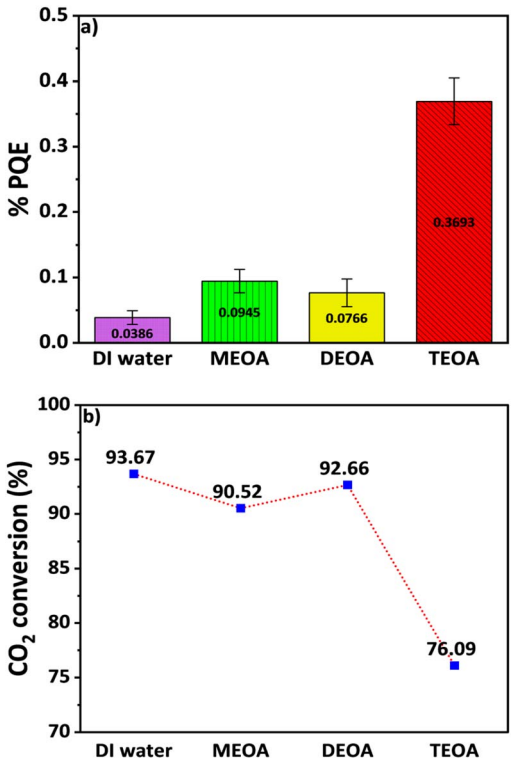

Fig. 3 (a) % PQE of the light source (160 W Hg lamp) on CO_2 photoreduction with different facilitators and (b) CO_2 conversion.

Photoluminescence (PL) spectroscopy

PL analysis determines the photoactivity of a photocatalyst by assessing its ability to be activated and emit light in the luminescence spectrum. CTGN was tested for its photoactivity in water and alkanolamines (Fig. 4) by being excited at 260 nm and monitored for photoemission within the 380–500 nm range during relaxation. The photoemission signal correlates with the electron–hole recombination phenomenon in the photocatalyst, where a strong signal indicates rapid recombination and poor photoactivity. We analyzed the photoemission signal by normalizing the signal intensity of the characteristic peak (wavelength = 429 nm) of alkanolamine to that of water and defined it as a quenching factor (QF, eqn (9)).[19]

$$QF = \frac{\text{PL signal intensity from alkanolamine}}{\text{PL signal from water}} \quad (9)$$

The QFs were 1.00, 0.79, 1.06, and 0.45 for CTGN with water, MEOA, DEOA, and TEOA, respectively. MEOA is a primary amine with high diffusivity and nucleophilicity, providing 21% lower QF than water. DEOA presents an equivalent QF to water, indicating a comparable SCR ability. TEOA assists CTGN better than water and the other alkanolamines, resulting in a QF that is 55% lower than that of water (as addressed further in the Discussion). PL analysis supported the results from CO_2 photoreduction since TEOA exhibited the best performance as a facilitator for the CTGN photocatalyst.

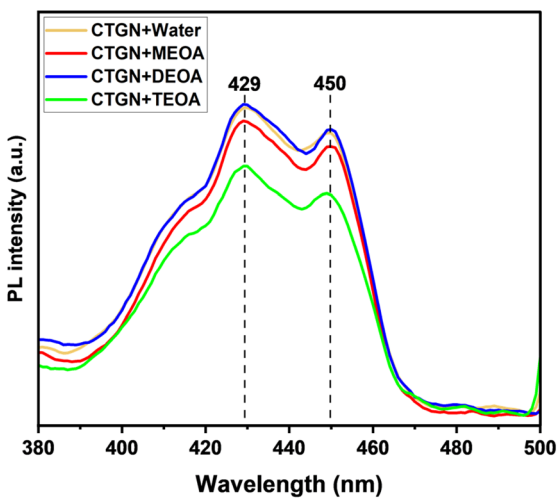

Fig. 4 PL spectra of CTGN with water and alkanolamines.

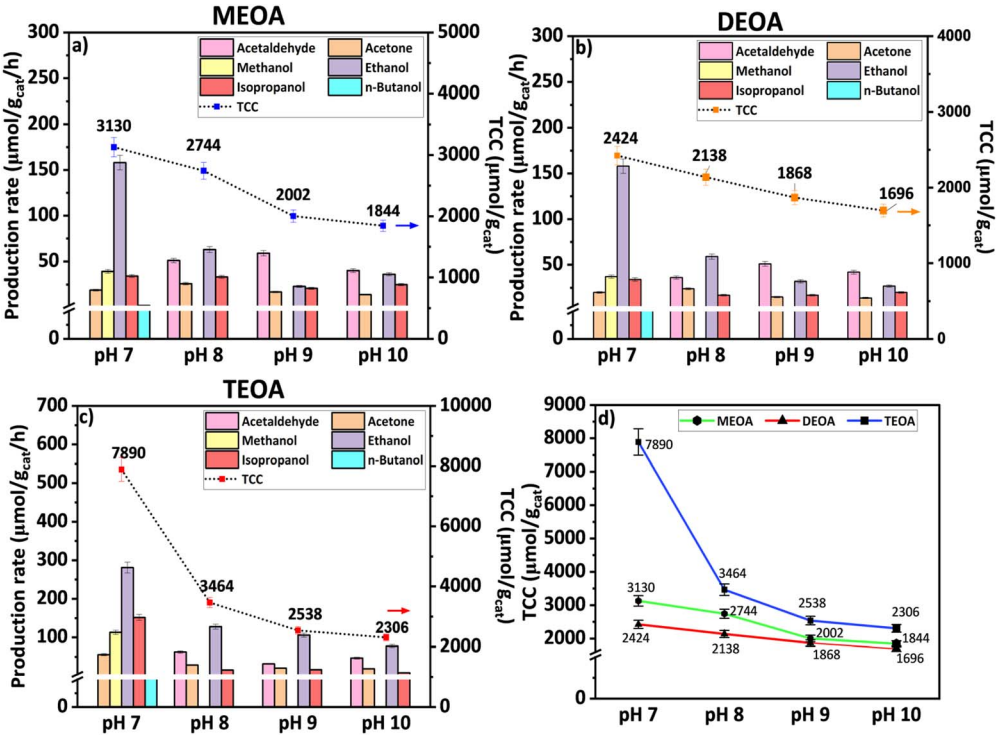

Fig. 5 Effect of pH on CO_2 photoreduction with (a) MEOA, (b) DEOA, (c) TEOA, and (d) overall ($n = 3$).

Effect of solution pH on CO_2 photoreduction

The effect of solution pH on CO_2 photoreduction was studied by adjusting the pH of the CTGN suspension after adding alkanolamine and CO_2 purging from ~7 to 8, 9, and 10, using NaOH solution.[33,34] For MEOA, at pH 8, the alkanolamine facilitated the generation of acetaldehyde, acetone, ethanol, and isopropanol at production rates of 51 ± 9, 26 ± 9, 63 ± 10, and 33 ± 2 μmol g_{cat}^{-1} h^{-1}, respectively (Fig. 5(a)). The TCC decreased from 3130 μmol g_{cat}^{-1} at pH 7 to 2744 μmol g_{cat}^{-1} at pH 8. At pH 9 and 10, the production rates were 59 ± 22, 17 ± 3, 23 ± 3, and 21 ± 6 μmol g_{cat}^{-1} h^{-1}, and 40 ± 5, 14 ± 0, 36 ± 1, and 25 ± 2 μmol g_{Cat}^{-1} h^{-1} for acetaldehyde, acetone, ethanol, and isopropanol, respectively. The TCC reduced from 2002 μmol g_{cat}^{-1} to 1844 μmol g_{cat}^{-1}, corresponding to a pH increase from 9 to 10. For DEOA (Fig. 5(b)), at pH 8, production rates for acetaldehyde, acetone, ethanol, and isopropanol were 36 ± 5, 24 ± 1, 59 ± 6, and 17 ± 4 μmol g_{cat}^{-1} h^{-1}, respectively. The TCC value dropped from 2424 μmol g_{cat}^{-1} (pH 7) to 2138 μmol g_{cat}^{-1} (pH 8). The production rates for pH 9 and 10 were 51 ± 7, 15 ± 1, 32 ± 3, and 17 ± 3 μmol g_{cat}^{-1} h^{-1} and 42 ± 6, 14 ± 3, 27 ± 3, and 20 ± 2 μmol g_{cat}^{-1} h^{-1} for acetaldehyde, acetone, ethanol, and isopropanol, respectively. The TCC dropped from 1868 μmol g_{cat}^{-1} at pH 9 to 1696 μmol g_{cat}^{-1} at pH 10. For TEOA (Fig. 5(c)), CO_2 photoreduction at pH 8 produced 63 ± 1, 29 ± 3, 128 ± 12, and 16 ± 4 μmol g_{cat}^{-1} h^{-1} acetaldehyde, acetone, ethanol, and isopropanol, respectively. The photoreduction at pH 9 and 10 yielded 32 ± 4, 21 ± 7, 106 ± 16, and 17 ± 0 μmol g_{cat}^{-1} h^{-1} and 47 ± 3, 19 ± 2, 78 ± 3, and 9 ± 3 μmol g_{cat}^{-1} h^{-1} acetaldehyde, acetone, ethanol, and isopropanol, respectively. The TCC at pH 8, 9, and 10 with TEOA were 3,464, 2,538, and 2306 μmol g_{cat}^{-1}, respectively. In all tests, the increase in pH resulted in a decrease in the product generation rate and TCC (Fig. 5(d)). The reduction in photoreduction rate can be attributed to the stronger bond between CO_2 and the hydroxyl ion (OH^-) and the lesser hole-scavenging ability of the SCR at higher pH levels (pH 8–10). The effect of CO_2 interactions with water, OH^-, and alkanolamine intensifies at a higher pH value, decreasing the CO_2 desorption rate and slowing down the subsequent CO_2 photoreduction.

Discussion

The CTGN was used as a photocatalyst model to study the effects of three alkanolamines, MEOA, DEOA, and TEOA, on supporting CO_2 photoreduction. The reaction mechanisms (Fig. 6) consist of four main steps: CO_2 capture (Fig. 6(I)), CO_2 desorption (Fig. 6(II)), active radical generation (Fig. 6(III)), and hole scavenging (Fig. 6(IV)). The CO_2 capture (I) occurs during CO_2 purging in the CTGN suspension with alkanolamine, creating a CO_2-saturated medium. For the CO_2 to be converted to target products, alkanolamine must desorb CO_2 (II) for the photoreduction, in which CO_2 couples with a photoelectron to become a CO_2^{*-} (III) radical. The radical reacted with other moieties in the suspension, becoming target products. The alkanolamines also approach CTGN, quench photo-induced holes (h^+) to protons (H^+) (IV), and become radicals themselves (eqn (10)–(12)). The radicals (MEOA*, DEOA*, and TEOA*) could later react with other intermediates available in the solution.

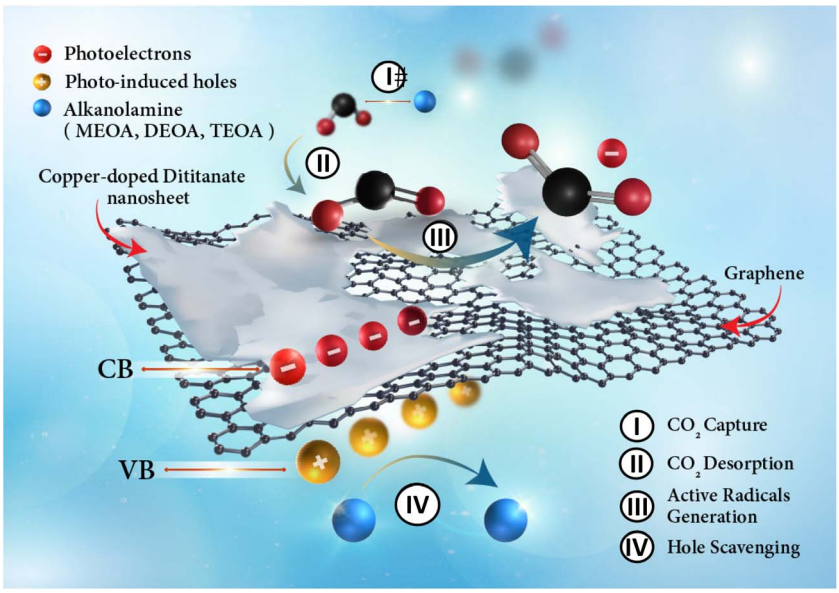

Fig. 6 Schematic diagram showing CO_2 photoreduction on the CTGN photocatalyst with alkanolamines.

$$MEOA + h^+ \rightarrow MEOA^* + H^+ \quad (10)$$

$$DEOA + h^+ \rightarrow DEOA^* + H^+ \quad (11)$$

$$TEOA + h^+ \rightarrow TEOA^* + H^+ \quad (12)$$

Results from CO_2 photoreduction revealed TEOA as the most effective facilitator for CTGN, providing a TCC of 7890 μmol g_{cat}^{-1}, compared to DEOA (2424 μmol g_{cat}^{-1}) and MEOA (3130 μmol g_{cat}^{-1}). The excellent performance of TEOA can be analyzed in terms of its two roles as a facilitator in CO_2 photoreduction: withdrawing photo-induced holes (SCR) and CO_2 capture. As an SCR, three factors were known to affect hole-scavenging ability: diffusivity, nucleophilicity, and relative permittivity (Table 1).[30,31] MEOA is a small molecule with a p*K*a of 9.44, providing higher diffusivity and more nucleophilicity than DEOA (p*K*a = 8.88) and TEOA (p*K*a = 7.76) (Table 1). Permittivity indicates the amount of electric charge contained in a molecule and its ability to stabilize other radicals, correlating with the hole-scavenging ability. MEOA displays a relative permittivity of 31.9, whereas DEOA and TEOA yield values of 25.8 and 29.3, respectively, indicating that MEOA is a more efficient SCR than TEOA and DEOA. The diffusivity, nucleophilicity, and permittivity trends contrast with the PL analysis, in which TEOA yielded the best hole-scavenging ability in the absence of CO_2. We prioritize the primary data from PL analysis and propose that functional groups can contribute to the hole-scavenging ability. Considering that the deprotonated hydroxyl group ($-O^-$) of alkanolamine helps stabilize photo-induced holes, TEOA with three $-O^-$ (Table 1), therefore, assists photocatalysts better than DEOA and MEOA with two and one $-O^-$, resulting in the enhanced CO_2 photoreduction rate.[35] Concerning the CO_2-capturing role, MEOA and DEOA react with CO_2 faster than TEOA due to the robust nature of the acid–base reaction (CO_2–MEAO and CO_2–DEOA) compared to the base-catalyzed hydration (CO_2–TEOA). TEOA also desorbs CO_2 quicker than MEOA and DEOA due to the weak CO_2–TEOA bond. The analysis supports the CO_2 photoreduction result, indicating the dominance of CO_2 desorption when TEOA is used. MEOA assists photoreduction better than DEOA as it is more nucleophilic than DEOA. The pH of the suspension contributes to the photoreduction rate and type of products. The initial pH for the CTGN suspension with no alkanolamine was ~7, and it reduced to ~5 with dissolved CO_2. The suspension with alkanolamines and dissolved CO_2 provided a pH of ~7. The target products were methanol, ethanol, isopropanol, acetone, and *n*-butanol, with ethanol being the primary product. As the suspension pH was adjusted to 8, 9, and 10, the TCC decreased, and the target products were acetaldehyde, ethanol, isopropanol, and acetone for CTGN suspension with alkanolamines. In the case of MEOA and DEOA, acetaldehyde and ethanol were the two major products. Ethanol production was higher than acetaldehyde at pH 8, but the trend reversed at pH 9 and 10. In the case of TEOA, ethanol and acetaldehyde were the major products, with the ethanol production rate exceeding that of acetaldehyde at pH 8, 9, and 10. The preference in product generation concerning the solution pH can be attributed to a balance between the CO_2–alkanolamine and CO_2–alkali interactions. More studies are needed to clarify this part. Our group previously tested the photoactivity of CTGN in catalyzing CO_2 photoreduction, relying on water and alcohol SCRs.[17,19] The photoreduction produced methane, acetaldehyde, methanol, ethanol, acetone, and isopropanol at TCCs ranging from 3426 to 6544 μmol g_{cat}^{-1}. Adding an alkanolamine to the CO_2-saturated CTGN suspension promotes product generation rates beyond those of the alcohols, yielding an enhanced TCC of 7890 μmol g_{cat}^{-1} in the case of TEOA. We realized a more extensive target product, *n*-butanol, due to the interactions between CO_2, intermediates, and alkanolamine.

Such interactions promoted CO_2 dissolution in water and stabilized intermediates, forming a bigger product for photoreduction. Total reactions for generation of the target products, acetaldehyde (C_2H_4O), methanol (CH_3OH), ethanol (C_2H_5OH), isopropanol (C_3H_7OH), acetone ($(CH_3)_2CO$), and *n*-butanol ($C_4H_{10}O$) are proposed here as follows (eqn (13)–(18)):

$$2CO_2 + 10H^+ + 10e^- \rightarrow C_2H_4O + 3H_2O \quad (13)$$

$$CO_2 + 6H^+ + 6e^- \rightarrow CH_3OH + H_2O \quad (14)$$

$$2CO_2 + 12H^+ + 12e^- \rightarrow C_2H_5OH + 3H_2O \quad (15)$$

$$3CO_2 + 18H^+ + 18e^- \rightarrow C_3H_7OH + 5H_2O \quad (16)$$

$$3CO_2 + 16H^+ + 16e^- \rightarrow (CH_3)_2CO + 5H_2O \quad (17)$$

$$4CO_2 + 24H^+ + 24e^- \rightarrow C_4H_{10}O + 7H_2O \quad (18)$$

The production of methanol, ethanol, isopropanol, and acetone, as mentioned in our previous study,[19] provided redox potentials (E^0_{redox}) of −0.38, −0.33, −0.31, and −0.36 V, respectively. The groups of Bertheussen E. (2016)[36] and Ting L.R. L. (2020)[37] reported the electroreduction potentials for CO_2 to acetaldehyde and *n*-butanol to be −0.33 and −0.48 V, respectively. The E^0_{redox} values suggest that photoreduction prefers isopropanol to ethanol, acetaldehyde, acetone, methanol, and *n*-butanol. This analysis contrasted with the experimental results, which revealed ethanol as the primary product with nearly equivalent production rates for methanol and isopropanol in all photoreductions with alkanolamine. This phenomenon indicates that other factors, such as intermediate formation pathways, contribute more significantly to the product type and generation rate.

Conclusions

This research highlighted the effects of three alkanolamines, MEOA, DEOA, and TEOA, on CTGN in CO_2 photoreduction. TEOA showed the best performance in supporting the CO_2 photoreduction, achieving products, including acetaldehyde, methanol, ethanol, isopropanol, acetone, and *n*-butanol with an impressive TCC of 7890 μmol g_{cat}^{-1}, compared to MEOA (3130 μmol g_{cat}^{-1}), DEOA (2424 μmol g_{cat}^{-1}), and water (2086 μmol g_{cat}^{-1}). The outstanding performance of TEOA was attributed to its impressive hole-scavenging ability and weak CO_2–TEOA interaction, which enabled rapid CO_2 desorption for subsequent photoreduction. In other studies, increased solution pH led to deceased TCC due to stronger bonds between CO_2 and the alkali solution. The bonds reduced the CO_2 desorption rate and, eventually, the CO_2 photoreduction rate. The work emphasizes the significance of alkanolamine as a facilitator for photocatalysts and its role in enhancing CO_2 photoreduction. Choosing a suitable facilitator for the reaction could increase the product generation rate and be a key factor in advancing CO_2 conversion technology.

Data availability

The data supporting this article have been included as part of the ESI.†

Author contributions

Wannisa Neamsung was responsible for conducting experiments, collecting raw data, and writing the first draft of the manuscript. Nutkamol Kitjanukit, Apisit Karawek, Napatr Chongkol, Napat Lertthanaphol, Poomipat Chotngamkhum, and Kongphoom Khumsupa contributed to data validation, as well as part of the experimental design and data analysis. Poomiwat Phadungbut, Woranart Jonglertjunya, and Pattaraporn Kim-Lohsoontorn assisted in data analysis and manuscript editing. Sira Srinives contributed to manuscript writing, graphic design, procuring funding, and supervising the project.

Conflicts of interest

The authors declare no financial or personal interest that affects professional judgment regarding the validity and analysis of this research.

Acknowledgements

The authors thank the Research CESS Fund, Malaysia-Thailand Joint Authority (MTJA), for financial support. We also acknowledge the assistance of the Mahidol University Frontier Research Facility (MUFRF) staff, researchers, and the Department of Chemical Engineering Central Lab for material characterization and analysis of CO_2 photoreduction product composition. Sira appreciates the contribution from the MU Talent Program, Faculty of Engineering, Mahidol University. Nutkamol is grateful to the 60th Year Supreme Reign of His Majesty King Bhumibol Adulyadej Scholarship for financial support.

References

1 V. Masson-Delmotte, P. Zhai, H. O. Pörtner, D. Roberts, J. Skea and P. R. Shukla, *Global Warming of 1.5 °C: IPCC Special Report on Impacts of Global Warming of 1.5 °C above Pre-industrial Levels in Context of Strengthening Response to Climate Change, Sustainable Development, and Efforts to Eradicate Poverty*, Cambridge University Press, 2022.

2 P. Panja, B. McPherson and M. Deo, Techno-economic analysis of amine-based CO_2 capture technology: hunter plant case study, *Carbon Capture Sci. Technol.*, 2022, **3**, 100041.

3 N. Sadeghi and M. Sillanpää, High selective photocatalytic CO_2 conversion into liquid solar fuel over a cobalt porphyrin-based metal-organic framework, *Photochem. Photobiol. Sci.*, 2021, **20**(3), 391–399.

4 T. Luo, Z. Wang, X. Han, Y. Chen, D. Iuga, D. Lee, B. An, S. Xu, X. Kang and F. Tuna, Efficient photocatalytic

reduction of CO_2 catalyzed by the metal-organic framework MFM-300 (Ga), *CCS Chem.*, 2022, **4**(8), 2560–2569.

5 R. Bouma, F. Vercauteren, P. Van Os, E. Goetheer, D. Berstad and R. Anantharaman, Membrane-assisted CO_2 liquefaction: performance modelling of CO_2 capture from flue gas in cement production, *Energy Procedia*, 2017, **114**, 72–80.

6 S. Cloete, M. N. Khan and S. Amini, Economic assessment of membrane-assisted autothermal reforming for cost effective hydrogen production with CO_2 capture, *Int. J. Hydrogen Energy*, 2019, **44**(7), 3492–3510.

7 D. Berstad, R. Anantharaman and P. Nekså, Low-temperature CO_2 capture technologies-Applications and potential, *Int. J. Refrig.*, 2013, **36**(5), 1403–1416.

8 D. K. De, I. A. Oduniyi and A. A. Sam, A novel cryogenic technology for low-cost carbon capture from NGCC power plants for climate change mitigation, *Therm. Sci. Eng. Prog.*, 2022, **36**, 101495.

9 M. Ali, N. K. Jha, N. Pal, A. Keshavarz, H. Hoteit and M. Sarmadivaleh, Recent advances in carbon dioxide geological storage, experimental procedures, influencing parameters, and future outlook, *Earth-Sci. Rev.*, 2022, **225**, 103895.

10 S. J. Altman, B. Aminzadeh, M. T. Balhoff, P. C. Bennett, S. L. Bryant, M. B. Cardenas, K. Chaudhary, R. T. Cygan, W. Deng and T. Dewers, Chemical and hydrodynamic mechanisms for long-term geological carbon storage, *J. Phys. Chem. C*, 2014, **118**(28), 15103–15113.

11 E. E. Adams and K. Caldeira, Ocean storage of CO_2, *Elements*, 2008, **4**(5), 319–324.

12 E. S. Sanz-Pérez, C. R. Murdock, S. Didas and C. W. Jones, Direct capture of CO_2 from ambient air, *Chem. Rev.*, 2016, **116**(19), 11840–11876.

13 M. Aggarwal, S. Basu, N. P. Shetti, M. N. Nadagouda and T. M. Aminabhavi, Photocatalytic conversion of CO_2 into valuable products using emerging two-dimensional graphene-based nanomaterials: A step towards sustainability, *Chem. Eng. J.*, 2021, **425**, 131401.

14 Y. Wang, E. Chen and J. Tang, Insight on reaction pathways of photocatalytic CO_2 conversion, *ACS Catal.*, 2022, **12**(12), 7300–7316.

15 L. Qiu-Ye, Z. Lan-Lan, L. Chen, C. Yu-Hui, W. Xiao-Dong and Y. Jian-Jun, Photocatalytic reduction of CO_2 to methane on Pt/TiO_2 nanosheet porous film, *Adv. Condens. Matter Phys.*, 2014, **2014**(1), 316589.

16 P. Seeharaj, N. Vittayakorn, J. Morris and P. Kim-Lohsoontorn, $CeO_2/CuO/TiO_2$ heterojunction photocatalysts for conversion of CO_2 to ethanol, *Nanotechnology*, 2021, **32**(37), 375707.

17 N. Kitjanukit, W. Neamsung, A. Karawek, N. Lertthanaphol, N. Chongkol, K. Hiramatsu, T. Sekiguchi, S. Pornsuwan, T. Sakurai and W. Jonglertjunya, Effects of alcohols as sacrificial reagents on a copper-doped sodium dititanate nanosheets/graphene oxide photocatalyst in CO_2 photoreduction, *RSC Adv.*, 2024, **14**(38), 27980–27989.

18 N. Lertthanaphol, N. Pienutsa, K. Chusri, T. Sornsuchat, P. Chanthara, P. Seeharaj, P. Kim-Lohsoontorn and S. Srinives, One-step hydrothermal synthesis of precious metal-doped titanium dioxide-graphene oxide composites for photocatalytic conversion of CO_2 to ethanol, *ACS Omega*, 2021, **6**(51), 35769–35779.

19 N. Lertthanaphol, N. Prawiset, P. Soontornapaluk, N. Kitjanukit, W. Neamsung, N. Pienutsa, K. Chusri, T. Sornsuchat, P. Chanthara and P. Phadungbut, Soft template-assisted copper-doped sodium dititanate nanosheet/graphene oxide heterostructure for photoreduction of carbon dioxide to liquid fuels, *RSC Adv.*, 2022, **12**(37), 24362–24373.

20 D. Mateo, A. M. Asiri, J. Albero and H. García, The mechanism of photocatalytic CO_2 reduction by graphene-supported Cu_2O probed by sacrificial electron donors, *Photochem. Photobiol. Sci.*, 2018, **17**, 829–834.

21 A. Karawek, K. Kittipoom, L. Tansuthepverawongse, N. Kitjanukit, W. Neamsung, N. Lertthanaphol, P. Chanthara, S. Ratchahat, P. Phadungbut and P. Kim-Lohsoontorn, The Photocatalytic Conversion of Carbon Dioxide to Fuels Using Titanium Dioxide Nanosheets/Graphene Oxide Heterostructure as Photocatalyst, *Nanomaterials*, 2023, **13**(2), 320.

22 A. Karawek, N. Kitjanukit, W. Neamsung, C. Kinkaew, P. Phadungbut, P. Seeharaj, P. Kim-Lohsoontorn and S. Srinives, Alkanolamine-Grafted and Copper-Doped Titanium Dioxide Nanosheets–Graphene Composite Heterostructure for CO_2 Photoreduction, *ACS Appl. Energy Mater.*, 2023, **6**(21), 10929–10942.

23 S. Srinives, T. Sarkar, R. Hernandez and A. Mulchandani, A miniature chemiresistor sensor for carbon dioxide, *Anal. Chim. Acta*, 2015, **874**, 54–58.

24 S. Likhittaphon, R. Panyadee, W. Fakyam, S. Charojrochkul, T. Sornchamni, N. Laosiripojana, S. Assabumrungrat and P. Kim-Lohsoontorn, Effect of CuO/ZnO catalyst preparation condition on alcohol-assisted methanol synthesis from carbon dioxide and hydrogen, *Int. J. Hydrogen Energy*, 2019, **44**(37), 20782–20791.

25 J. Schneider and D. W. Bahnemann, Undesired role of sacrificial reagents in photocatalysis, *J. Phys. Chem. Lett.*, 2013, **4**(20), 3479–3483.

26 J. Sun, W. Liu, W. Wang, Y. Hu, X. Yang, H. Chen, Y. Peng and M. Xu, CO_2 sorption enhancement of extruded-spheronized CaO-based pellets by sacrificial biomass templating technique, *Energy Fuels*, 2016, **30**(11), 9605–9612.

27 Y. Pellegrin and F. Odobel, Sacrificial electron donor reagents for solar fuel production, *C. R. Chim.*, 2017, **20**(3), 283–295.

28 Y. Liao, S. W. Cao, Y. Yuan, Q. Gu, Z. Zhang and C. Xue, Efficient CO_2 capture and photoreduction by amine-functionalized TiO_2, *Chem.–Eur. J.*, 2014, **20**(33), 10220–10222.

29 Y. E. Kim, J. A. Lim, S. K. Jeong, Y. I. Yoon, S. T. Bae and S. C. Nam, Comparison of carbon dioxide absorption in aqueous MEA, DEA, TEA, and AMP solutions, *Bull. Korean Chem. Soc.*, 2013, **34**(3), 783–787.

30 E. Ikada, Y. Hida and H. Okamoto, Dielectric properties of ethanolamines, *Bull. Inst. Chem. Res., Kyoto Univ.*, 1968, **46**(5), 239–247.

31 M. Wang, S. Shen, L. Li, Z. Tang and J. Yang, Effects of sacrificial reagents on photocatalytic hydrogen evolution over different photocatalysts, *J. Mater. Sci.*, 2017, **52**, 5155–5164.
32 H.-Y. Wu, H. Bai and J. C. Wu, Photocatalytic reduction of CO_2 using Ti–MCM-41 photocatalysts in monoethanolamine solution for methane production, *Ind. Eng. Chem. Res.*, 2014, **53**(28), 11221–11227.
33 T. Nguyen Thi Thu, N. Nguyen Thi, V. Tran Quang, K. Nguyen Hong, T. Nguyen Minh and N. Le Thi Hoai, Synthesis, characterisation, and effect of pH on degradation of dyes of copper-doped TiO_2, *J. Exp. Nanosci.*, 2016, **11**(3), 226–238.
34 M. Du, Effect of pH on desorption of CO_2 from alkanolamine-rich solvents, *AIP Conf. Proc.*, 2017, **1864**(1), 020091.
35 U. Pal, S. Ghosh and D. Chatterjee, Effect of sacrificial electron donors on hydrogen generation over visible light–irradiated nonmetal-doped TiO_2 photocatalysts, *Transition Met. Chem.*, 2012, **37**, 93–96.
36 E. Bertheussen, A. Verdaguer-Casadevall, D. Ravasio, J. H. Montoya, D. B. Trimarco, C. Roy, S. Meier, J. Wendland, J. K. Nørskov, I. E. L. Stephens and I. Chorkendorff, Acetaldehyde as an Intermediate in the Electroreduction of Carbon Monoxide to Ethanol on Oxide-Derived Copper, *Angew. Chem., Int. Ed.*, 2016, **55**, 1450–1454.
37 L. R. L. Ting, R. García-Muelas, A. J. Martín, F. L. P. Veenstra, S. T. J. Chen, Y. Peng, E. Y. X. Per, S. Pablo-García, N. López, J. Perez-Ramírez and B. S. Yeo, Electrochemical Reduction of Carbon Dioxide to 1-Butanol on Oxide-Derived Copper, *Angew. Chem., Int. Ed.*, 2020, **59**, 21072–21079.